Materials Science and Engineering C 59 (2016) 611–616

Contents lists available at ScienceDirect

Materials Science and Engineering C

journal homepage: www.elsevier.com/locate/msec

# Cell adhesion on NiTi thin film sputter-deposited meshes

K. Loger [a,1], A. Engel [b,1], J. Haupt [b], Q. Li [c], R. Lima de Miranda [a,d], E. Quandt [a], G. Lutter [b], C. Selhuber-Unkel [c,*]

[a] Inorganic Functional Materials, Institute for Materials Science, Faculty of Engineering, University of Kiel, Germany
[b] Department of Cardiovascular Surgery, University Hospital of Schleswig-Holstein, Kiel, Germany
[c] Biocompatible Nanomaterials, Institute for Materials Science, Faculty of Engineering, University of Kiel, Germany
[d] ACQUANDAS GmbH, Kiel, Germany

ARTICLE INFO

*Article history:*
Received 17 July 2015
Received in revised form 10 September 2015
Accepted 2 October 2015
Available online 13 October 2015

*Keywords:*
NiTi
Thin film scaffold
Sputter deposition
Mechanical properties
Cell adhesion
Shape memory alloy

ABSTRACT

Scaffolds for tissue engineering enable the possibility to fabricate and form biomedical implants in vitro, which fulfill special functionality in vivo. In this study, free-standing Nickel–Titanium (NiTi) thin film meshes were produced by means of magnetron sputter deposition. Meshes contained precisely defined rhombic holes in the size of 440 to 1309 μm$^2$ and a strut width ranging from 5.3 to 9.2 μm. The effective mechanical properties of the microstructured superelastic NiTi thin film were examined by tensile testing. These results will be adapted for the design of the holes in the film. The influence of hole and strut dimensions on the adhesion of sheep autologous cells (CD133+) was studied after 24 h and after seven days of incubation. Optical analysis using fluorescence microscopy and scanning electron microscopy showed that cell adhesion depends on the structural parameters of the mesh. After 7 days in cell culture a large part of the mesh was covered with aligned fibrous material. Cell adhesion is particularly facilitated on meshes with small rhombic holes of 440 μm$^2$ and a strut width of 5.3 μm. Our results demonstrate that free-standing NiTi thin film meshes have a promising potential for applications in cardiovascular tissue engineering, particularly for the fabrication of heart valves.



## 1. Introduction

The development of new scaffolds for tissue engineering is a challenging task that has become of increasing interest in the last decade. The mechanical properties of such scaffolds and their design are known to strongly affect cell growth, the formation and integration of extracellular matrix proteins and the functionality of the device as a whole [1]. A tissue engineering approach in general for generating biomedical implants has various promising applications. This is particularly the case for bioprosthetic cardiovascular implants. The major issues of conventional bioprosthetic heart valves, such as xenografts, are the limited durability due to re-calcification.

NiTi is a widely used material for many implant types such as stents, septal occluders or vena cava filters [2]. Due to its superelastic properties it is well suited for transcatheter-based implants. The implant regains its initial shape when it is deployed from the catheter so that no balloon expansion system is needed. Further studies proved the excellent biocompatibility of NiTi material [3–5]. NiTi thin film technology allows the fabrication of complex geometrical structures with micrometer precision from materials with high cyclic mechanical stability [6]. In this regard, NiTi has already demonstrated great potential as a biomaterial for heart valve leaflets [7,8].

Before applying such materials for in vivo applications, biocompatibility and cell growth must be guaranteed. It is a well-studied phenomenon that cell adhesion can be controlled geometrically by 2D micropatterns of extracellular matrix proteins. Such patterns are often generated either with microcontact printing [9] or by using bottom-up approaches [10,11]. On such protein micropatterns it is possible to control cell life and death by pattern geometry [12] and to influence cell shape, focal adhesion and actin stress fiber formation [13]. In addition, not only the size and micropattern of a cell-adhesive area are responsible for the ability of a cell to spread on a substrate, but also the nanoscale spacing of single cell adhesion ligands [14,15]. A further important role has been attributed to surface microtopography. Several studies have shown that cell adhesion, spreading and even tissue morphogenesis can be influenced by 2D micropillar structures [16]. Such micropillars can be fabricated from silicon elastomers and cell behavior is co-regulated by substrate topography and pillar bending stiffness [17,18].

Common approaches to generate materials for cardiovascular tissue engineering include cell seeded non-biological scaffolds as well as decellularized donor tissue. Decellularized native porcine heart valves seeded with CD133+ cells have shown good functionality in pulmonary valved stent implantation [19]. A further strategy to generate cardiovascular scaffolds by tissue engineering is the use of electrospun materials [20,21]. For example, Hinderer et al. studied the influence of electrospun poly-(L-lactide) scaffolds on valvular endothelial cells (VECs) and valvular interstitial cells (VICs) for bio-functionalized hybrid

* Corresponding author.
[1] These authors contributed equally to this work.

http://dx.doi.org/10.1016/j.msec.2015.10.008

heart valves [22]. Electrospun scaffolds made from poly(glycerol sebacate) and poly(ε-caprolactone) are also materials suitable for generating tissue engineered heart valves [23].

Compared to such polymer based tissue engineering approaches, a sputtered thin film NiTi based scaffold has the advantage of well-defined geometrical structures, uniform hole sizes and controllable effective mechanical properties as well as thinner structures for the same mechanical integrity.

In a recent study, Alavi et al. have reported on a hybrid heart valve leaflet based on a superelastic NiTi mesh core [24]. The NiTi scaffold was 76 μm thick and the mesh structure was acid etched, leading to a network of circular holes with a diameter of 240 μm and a central distance of 320 μm. This scaffold could be completely enclosed with a multi-layer of biological tissue. This work proved the suitability of NiTi scaffolds for biological applications in general. An examination of the inflammatory response found a lower TNF-α level for tissue enclosed meshes than for bare NiTi meshes, and furthermore, the superior biocompatibility of NiTi compared to stainless steel was confirmed.

In this study we characterized NiTi thin film meshes that contain rhombic holes. Mechanical properties were strongly related to the size of the holes and struts in the mesh, as well as on their orientation. In order to investigate the biological impact of these NiTi meshes, the adhesion of autologous progenitor cells (CD133+) on different NiTi meshes was studied. Cells adhering to the meshes were investigated at two different time points after 24 h and after seven days of incubation, using fluorescence microscopy and scanning electron microscopy (SEM), demonstrating the biocompatibility of the samples and the dependence of cell growth on the hole and strut dimensions.

## 2. Materials and methods

### 2.1. Fabrication of structured nickel–titanium thin films

NiTi thin film samples were fabricated by means of magnetron sputtering with an Alcatel 450 sputtering device on a silicon substrate. In order to attain freestanding films, NiTi films were deposited on a pre-sputtered Copper (Cu) sacrificial layer. Sputtering was carried out at a base pressure below $1 \times 10^{-7}$ mbar, an Argon flow of 20 sccm and a sputtering pressure of $2 \times 10^{-3}$ mbar. The magnetron sputtered films have a composition of $Ni_{50.5}Ti_{49.5}$ atom %. UV lithography and wet etching were performed to pattern NiTi thin film meshes and to attain freestanding films. The detailed process flow chart of the process and the wet etching procedure were described by Lima de Miranda et al. [25].

Rapid thermal annealing (RTA) with a heating rate of 50 K/s was used at 650 °C for 10 min to crystallize the amorphous NiTi. In detail, RTA was carried out in a vacuum environment at a pressure of about $10^{-7}$ to $10^{-6}$ mbar to avoid oxidation of the samples during heating. An additional aging step at 450 °C for 10 min, which is a common procedure to induce $Ti_3Ni_4$ precipitates in order to adjust the austenite to martensite phase transition temperature was also applied. The resulting austenite finish temperatures of 26.4 ± 0.9 °C were determined by differential scanning calorimetry. Thin film samples were fabricated as so-called dog bone structures with a thickness of 10 μm, having a rhombic hole mesh structure in their central rectangle, which had a length of 4.5 mm and a width of 2 mm (Fig. 1). Three different mesh sizes were fabricated, which are denoted as small (S), medium (M) and large (L). Characteristic sizes of the meshes are presented in Table 1.

### 2.2. Tensile test

Mechanical tests were performed in a Zwick/Roell Z0.5 tensile test device at a temperature of 37 °C. In order to gain information on the tensile properties of the NiTi thin film scaffolds, samples were characterized with the long axis of the rhombic mesh structure oriented parallel and perpendicular to the pulling direction, respectively. Tensile tests were carried out at a constant strain rate of 0.8%/min.

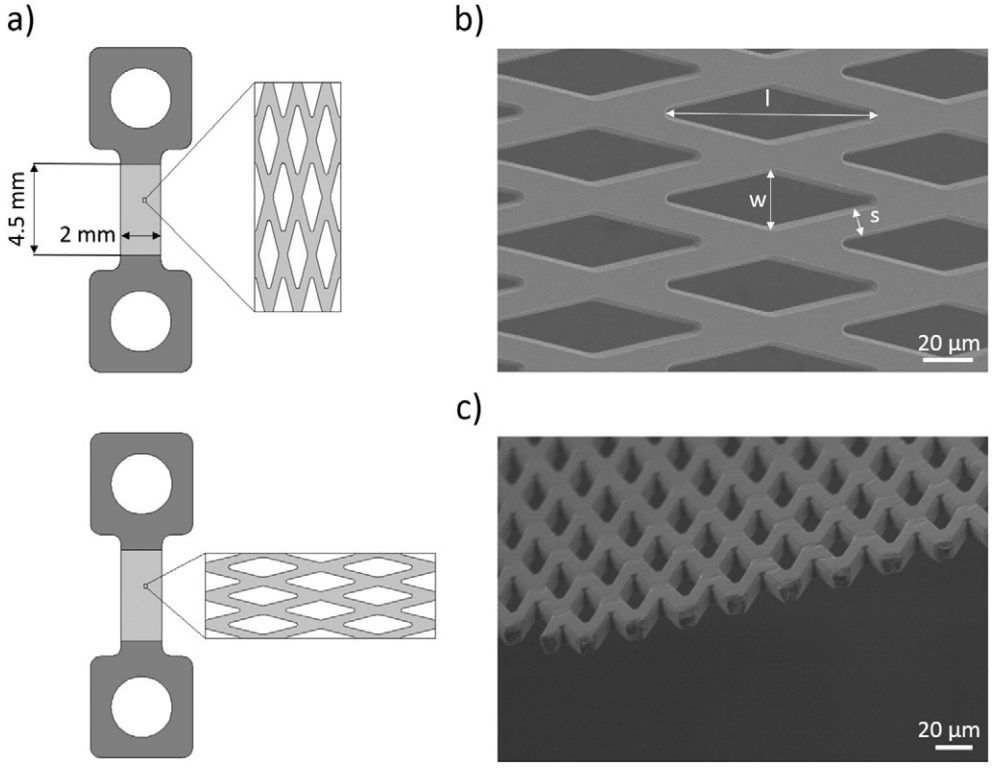


**Fig. 1.** Sample design: a) Transversally and longitudinally oriented rhombic dogbone structure with a parallel length of 4.5 mm and a width of 2 mm. b) Micrograph of the rhombic holes in the mesh with the rhombic length l, rhombic width w and the strut size s. Characteristic scaffold strut and rhombic hole sizes of freestanding NiTi meshes are given in Table 1. Thin film technology enables a mesh fabrication with precise rhombic hole and strut sizes throughout the whole scaffold. c) Fractured longitudinal NiTi thin film mesh.

**Table 1**
Strut width and rhombic hole size of differently sized NiTi mesh scaffolds, determined from SEM micrographs (Fig. 1). Due to the chamfers at the hole edges and the rounded hole corners, the hole geometry differs from a perfect rhomb and therefore the measured rhombic hole size is larger than the theoretical size determined from the rhombic width and length. S (Small), M (Medium) and L (Large) denote the different structure sizes of the meshes.

| Structure | S | M | L |
|---|---|---|---|
| Strut width s/μm | 5.3 ± 0.2 | 7.5 ± 0.2 | 9.2 ± 0.2 |
| Rhombic width w/μm | 15.1 ± 0.1 | 19.7 ± 0.2 | 24.7 ± 0.2 |
| Rhombic length l/μm | 45.0 ± 0.2 | 64.2 ± 0.1 | 84.5 ± 0.2 |
| Rhombic hole size/μm$^2$ | 440 ± 8 | 820 ± 21 | 1309 ± 37 |

### 2.3. Cell harvest

5 ml of bone marrow from juvenile sheep (shropshire breed) were diluted with phosphate-buffered saline (PBS, Biochrom AG Germany) and layered onto Ficoll (Lymphprep ™ AXIS-SHIELD PoC AS; Oslo, Norway). The cultured mononuclear cells (MNCs) were washed with PBS and $10^5$ CD133+ cells were isolated by using anti-CD133+ (Miltenyi) and the EasySep® Positive Selection Kit (Stemcell Technologies). The harvested cells were cultured in a fibronectin precoated 96-well plate with special precursor cell medium (Hemato Stem S Kit; PAA) [26,27].

### 2.4. Cell adhesion assays

Cells were maintained in Dulbecco's Modified Eagle's medium (DMEM, Biochrom, Germany), supplemented with 10% fetal bovine serum (FBS, Biochrom, Germany), 1% penicillin and streptomycin (100 U/ml, Biochrom, Germany) and 5 ng/ml fibroblast growth factor (FGF, PeproTech, Germany) at 37 °C, with 5% $CO_2$ and 90% humidity. Regular subculturing was carried out with 0.25% trypsin/0.05% ethylendiamine tetraacetic acid (EDTA, Biochrom, Germany) and cells were used up to passage 10.

For cell adhesion experiments, NiTi samples were mounted on a custom-built PTFE holder to guarantee that cells adhere to the free-standing NiTi mesh without simultaneous contact with the petri dish. Each teflon holder is made of four cantilevers with holding knobs and can hold up to four samples in parallel. The whole setup was put into a 4-chamber plate (Greiner bio-one, Germany).

### 2.5. Short-term cell adhesion assay

Cells were counted with a Neubauer chamber and $4 \times 10^4$ cells/cm$^2$ were seeded onto the NiTi sample in each chamber with 11.5 ml culture medium and incubated at 37 °C and 5% $CO_2$ (Binder, C150) for 24 h before checking their morphology. The samples were first washed once with DMEM and then incubated with calcein AM (2 μg/ml, BD Science, Germany) for 10 min at 37 °C. After a gentle washing procedure with PBS, that side of the NiTi samples, on which the cells had been seeded, was imaged with fluorescence microscopy (BX43, Olympus, Germany). To take a closer look at the cells, samples were fixed with 4% PFA (Sigma-Aldrich, Germany) at room temperature for 25 min. After washing twice with phosphate buffered saline (PBS), samples were placed into a specimen with vectashield (Vector Laboratories, USA) and investigated with fluorescence microscopy (IX 81, Olympus, Germany).

### 2.6. Long-term cell adhesion assay

Cell counting was carried out with a Neubauer counting chamber and cells were added on the NiTi structures at a density of $10^5$ cells/cm$^2$. Samples were incubated in Dulbecco's Modified Eagle's Medium (DMEM, Gibco Life Technologies) supplemented with 10% fetal calf serum (FCS, Gibco Life Technologies), 2% penicillin/streptomycin (Biochrom AG Germany), and 5 ng/ml FGF (PeproTech)

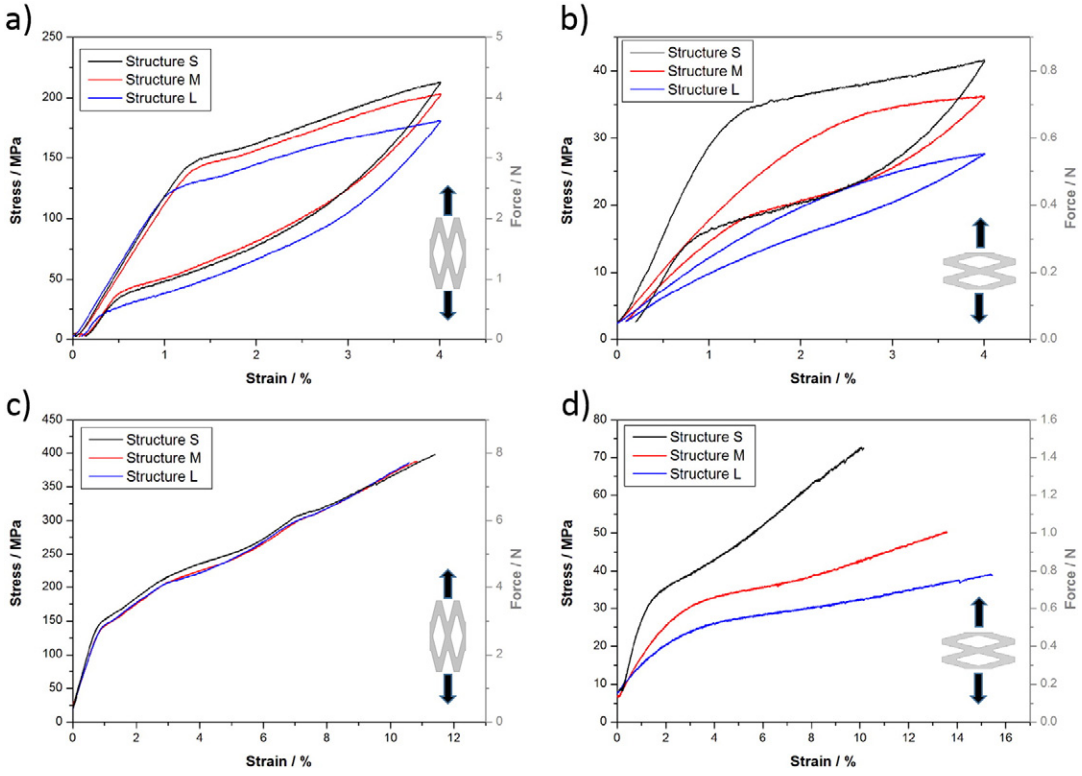


**Fig. 2.** Tensile tests of meshed NiTi scaffolds. a) Longitudinal pulling direction with 4% strain. b) Transversal pulling direction with 4% strain. The plateau shows the stress induced martensitic transformation of the material. c) Longitudinal fracture strain. d) Transversal fracture strain. The samples have an austenite finish temperature of 26.4 ± 0.9 °C and measurements were carried out at a testing temperature of 37 °C.

**Table 2**
Effective mechanical properties of different freestanding NiTi matrix scaffolds with different feature size (S, M, L) and mesh orientation. For comparison the mechanical properties of a non-structured NiTi thin film are provided.

| Mesh orientation | Longitudinal | | | Transversal | | | Full film |
|---|---|---|---|---|---|---|---|
| Structure | S | M | L | S | M | L | |
| Effective Young's modulus/GPa | 44.5 ± 1.2 | 43.4 ± 1.2 | 44.2 ± 1.2 | 10.6 ± 0.3 | 5.5 ± 0.2 | 3.6 ± 0.1 | 81.9 ± 2.2 |
| Effective tensile strength/MPa | 398 | 386 | 385 | 72 | 50 | 39 | 1480 |
| Fracture strain/% | 11.4 | 10.8 | 10.6 | 10.1 | 13.6 | 15.5 | 20.4 |

for 7 days at 37 °C and 5% $CO_2$ (Heraeus, Heracell 150). The medium was renewed every third day.

To visualize living cells on the NiTi mesh structures, calcein-acetoxymethyl ester (calcein-AM, BD Biosciences) staining with standard procedures described by R.E. Unger et al. was used [28]. The cell growth medium was replaced by a medium supplemented with 0.1 mM calcein-AM. After 30 min incubation at 37 °C the staining solution was replaced with PBS. The stained specimens were examined by confocal laser scanning microscopy (Leica TCS NT).

### 2.7. Scanning electron microscopy

Samples were washed with PBS for 5 min and dehydrated with alcohol at ascending concentrations up to 100% to remove excess water. Samples were dried following a critical-point drying procedure (CPD) described by Scherge et al. [29]. To enhance the conductivity, a 10 nm thin Au/Pd layer was sputtered on the samples. SEM micrographs were made with the Hitachi S-4800 at 3 kV.

## 3. Results

### 3.1. Mechanical properties

The geometric parameters of the different freestanding rhombic mesh structures were determined from SEM micrographs (Fig. 1, Table 1). Tensile test samples were prepared with the long axis of the rhombic holes oriented longitudinally and transversally to the pulling direction in order to compare the mechanical properties of the thin film in both directions (Fig. 2).

After applying a total strain of 4%, all transversally and longitudinally oriented samples regained their initial shape upon unloading at a testing temperature of 37 °C. The superelastic plateau shows the stress induced martensitic transformation of the NiTi material and has a length of about 3%, depending on the mesh structure. The total strain results from an interaction of the superelastic properties of the NiTi material and the structured geometry. In longitudinal strain direction, no significant dependence of the force-strain behavior on mesh sizes could be observed (Table 2). Tensile tests on transversally oriented scaffolds showed a mesh size dependent behavior. Smaller feature size induces a higher effective elastic modulus. With increasing mesh feature size the effective Young's modulus decreases from 10.6 ± 0.3 GPa to 3.6 ± 0.1 GPa. A similar decrease was observed for the total tensile strength. On the other hand, the fracture strain of transversally oriented meshes increased with bigger feature size from 10.1% to 15.5%. The plateau of the stress induced martensitic transformation is not as distinct for structures M and L in transversal direction. This indicates an increasing flexibility and higher ability for deformation of the transversally oriented mesh of structures M and L. Due to the structuring of the NiTi films and thus resulting in less NiTi material in the total cross section of the sample, the effective Young's modulus and the effective tensile strength are much smaller compared to non-structured NiTi film (Young's modulus of 81.9 GPa and tensile strength of 1480 MPa). An additional influence of shear stress on the struts as well as the rhombic shape design of the structured films leads to a lower fracture strain of the structured film compared to the full film material.

### 3.2. Short-term cell adhesion on NiTi micromeshes

Fig. 3 shows CD133 + cells seeded onto NiTi meshes and stained with calcein AM after 24 h of incubation. The number of cells adhering to meshes with small strut width and small hole size is larger than on meshes with large strut width and large hole size (Fig. 3A, B). Fig. 3C shows cells after additional fixation on a mesh with large strut width and large pore size. Clearly, cells can grow on the meshes in different configurations, for example along the struts or by bridging the holes. In general, adhesion to the NiTi meshes was very weak in this short-term adhesion experiment, as the washing steps during fixation removed a considerable number of cells and sometimes only cell remnants remain on the surface of the mesh.

### 3.3. Long-term cell adhesion on NiTi micromeshes

Fluorescence microscopy analysis after 7 days revealed a vital CD133 + cell layer on all NiTi mesh structures. Cell density differs for the different mesh structures. Structure S (Fig. 4A) shows the highest density followed by structure M (Fig. 4B). Structure L (Fig. 4C) reveals the lowest cell density. It becomes apparent that the NiTi structure with the smallest holes is better colonized than the structure with larger holes.

Fig. 5 shows an SEM image of CD133 + cells cultured for 7 days on a NiTi scaffold sample with structure S. The NiTi micromesh is covered with a dense layer of cellular fibrous material.

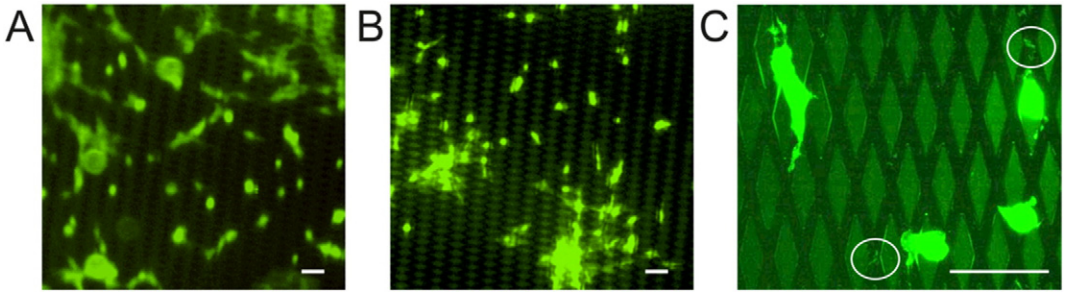


**Fig. 3.** CD133 + cells (green) stained with Calcein AM on NiTi meshes after 24 h of incubation. Scalebars: 100 μm. A: Living cells on structure S. B: Living cells on structure L. C: Higher magnification image of cells on structure L after additional fixation. Cells grow either along the struts (upper left corner) or across the pores of the mesh. After fixation fluorescent cell remnants are detected on the substrate (circles).

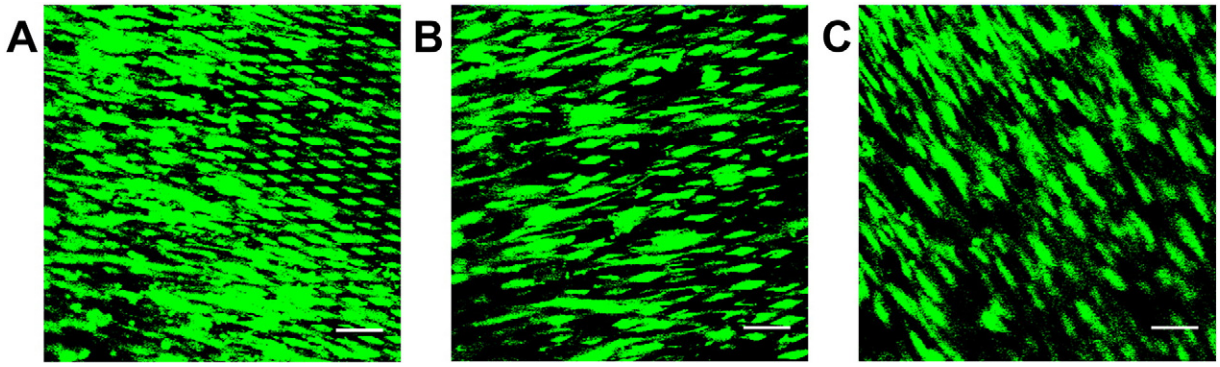


**Fig. 4.** CD133 + cells (green) stained with Calcein AM on NiTi meshes after seven days of incubation. A: Cells on structure S. B: Cells on structure M. C: Cells on structure L. The samples are seeded one sided. Both sample sides were investigated. Cells are growing on both sides of the samples, covering the black NiTi grid partially. Scalebars: 100 μm.

The fibers are mainly aligned along the longitudinal direction of the rhombic holes. They are even growing across the holes and covering them, so that the micromesh structure is enclosed. Approximately 70% of the mesh surface is covered with this fibrous material.

## 4. Discussion

The development of mechanically well-defined biocompatible materials is an important task in order to generate long-lasting, non-immunogenic and non-thrombogenic matrices for tissue engineered cardiovascular implants. In contrast to mechanically relatively soft materials with elasticities in the MPa regime, sputtered NiTi-based materials are highly promising due to their superelasticity, their mechanical long-term stability and excellent corrosion resistance [6,30].

Whereas the precise structural design of etched NiTi meshes and electrospun polymeric scaffolds cannot completely be controlled, we here demonstrate that the NiTi thin film sputtering process allows complex microscale designs of NiTi meshes with a high aspect ratio of the structures and precise thickness control of the micro meshes (Fig. 1). Furthermore, as shown in Table 2 and Fig. 2, the mechanical properties of the NiTi meshes are well-defined and can be adapted by varying the size and orientation of the integrated rhombic holes. Using cell adhesion assays we have shown that CD133 + cells can grow on the NiTi meshes, without regard for the specific mesh structures. Still, structures with small strut width and small hole size show a higher number of cells adhering on the NiTi scaffolds after 24 h (Fig. 3). Cells are able to grow along the struts, but will also cover the holes, which is e.g. a prerequisite for the use of these structures as heart valve leaflets. The adhesion of cells was initially weak as demonstrated by short term experiments but was found to be much stronger after an incubation of seven days. Fluorescence images after seven days revealed a confluent cell layer for the small NiTi mesh structure S and an almost confluent layer for structures M and L (Fig. 4). Since CD133 + cells are forming cell monolayers, the confluence after seven days indicates an increase in cell adhesion compared to experiments carried out after 1 day of incubation, as after 7 days cells did not significantly detach during the washing procedure.

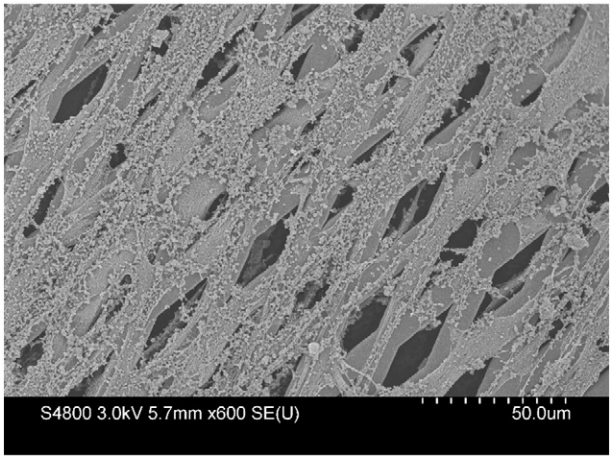


**Fig. 5.** SEM image of CD133 + cells NiTi mesh structure S. Fibers are clearly visible and mainly aligned along the longitudinal direction of the rhombic holes.

The SEM micrograph shows a sample covered with fibrous material after seven days. The NiTi thin film matrix has an influence on the fiber growth, as the fibers preferably grow along the long axis of the rhombic scaffold structure (Fig. 5). This is reminiscent of results received from micro-contact printed ECM proteins, where the geometry of the ECM micropattern guided the growth direction and orientation of cytoskeletal fibers [13]. Compared to controlling cell behavior by micropillar surfaces [18], we here assume that cell behavior is not influenced by the elasticity of the mesh, as NiTi has a much higher Young's modulus than materials that are known to influence cell behavior [31]. Instead, our results demonstrate that cell adhesion is regulated by the size of the holes and struts presented by the NiTi mesh.

## 5. Conclusions

We have shown that NiTi thin film meshes are promising biomaterials for the fabrication of mechanically and geometrically well-defined, free-standing tissue engineered cardiovascular implants. The effective mechanical properties of the scaffold can be adapted to the implant requirements by varying the hole and strut size and the macroscopic dimensions of the NiTi film. The NiTi thin film meshes are highly biocompatible and cell adhesion is controlled by the size of the rhombic holes in the mesh. All these properties together highlight the suitability of the NiTi thin film meshes for hybrid tissue engineered implants in heart valve applications, where the material must be able to withstand high shear stresses during blood flow and exhibit high flexibility to ensure high movability and good opening and closing properties of the valve leaflets. Furthermore, a confluent cell growth on the scaffold will lead to sufficient hybrid leaflets, avoiding blood to flow back through the closed valve.

## Acknowledgments

Project funding by the Deutsche Forschungsgemeinschaft is gratefully acknowledged (QU 146/11-1 and LU 663/11-1). Q. Li and C. Selhuber-Unkel acknowledge the ERC for funding through starting grant no. 336104. G. Lutter is gratefully supported by DZHK (German Centre for Heart and Circulation) through grant NCCR 3.4 HF. We thank Katharina Siemsen for support with the cell adhesion

experiments and the group of Functional Morphology and Biomechanics at the University of Kiel for support with the SEM experiments.

## Appendix A. Supplementary data

Supplementary data to this article can be found online at http://dx.doi.org/10.1016/j.msec.2015.10.008.

## References

[1] X. Ren, Y. Feng, J. Guo, H. Wang, Q. Li, J. Yang, X. Hao, J. Lv, N. Ma, W. Li, Surface modification and endothelialization of biomaterials as potential scaffolds for vascular tissue engineering applications, Chem. Soc. Rev. (2015).
[2] A. Meltzer, D. Stoeckel, Function and performance of nitinol vascular implants, Open Med. Dev. J. 2 (2) (2010) 32–41.
[3] J. Ryhänen, Biocompatibility Evolution of Nickel–Titanium Shape Memory Alloy, Faculty of Medicine, University of Oulu, Finland, 1999.
[4] S. Shabalovskaya, Surface, corrosion and biocompatibility aspects of nitinol as an implant material, Bio-Med. Mater. Eng. 12 (1) (2002) 69–109.
[5] T. Habijan, R. Lima de Miranda, C. Zamponi, E. Quandt, C. Greulich, T. Schildhauer, M. Köller, The biocompatibility and mechanical properties of cylindrical NiTi thin films produced by magnetron sputtering, Mater. Sci. Eng. C 32 (8) (2012) 2523–2528.
[6] G. Siekmeyer, A. Schüßler, R. Lima de Miranda, E. Quandt, Comparison of the fatigue performance of commercially produced samples versus sputter-deposited NiTi, J. Mater. Eng. Perform. 23 (7) (2014) 2437–2445.
[7] L. Stepan, D. Levi, G. Carman, A thin film nitinol heart valve, J. Biomech. Eng. 127 (6) (2005) 915–918.
[8] K. Loger, R. Lima de Miranda, A. Engel, M. Marczynski-Bühlow, G. Lutter, E. Quandt, Fabrication and evaluation of nitinol thin film heart valves, Cardiovasc. Eng. Technol. 5 (4) (2014) 308–316.
[9] A. Bernard, J. Renault, B. Michel, H. Bosshard, E. Delamarche, Microcontact printing of proteins, Adv. Mater. 12 (14) (2000) 1067–1070.
[10] D. Aydin, M. Schwieder, I. Louban, S. Knoppe, J. Ulmer, T. Haas, H. Walczak, J. Spatz, Micro-nanostructured protein arrays: a tool for geometrically controlled ligand presentation, Small 5 (9) (2009) 1014–1018.
[11] R. Piner, J. Zhu, F. Xu, S. Hong, C. Mirkin, "Dip-pen" nanolithography, Science 283 (661) (1999) 661–663.
[12] C. Chen, M. Mrksich, S. Huang, G. Whitesides, D. Ingber, Geometric control of cell life and death, Science 276 (1425) (1997) 1425–1428.
[13] M. Théry, A. Pépin, E. Dressaire, Y. Chen, M. Bornens, Cell distribution of stress fibres in response to the geometry of the adhesive environment, Cell Motil. Cytoskeleton 63 (6) (2006) 341–355.
[14] J. Deeg, I. Louban, D. Aydin, C. Selhuber-Unkel, H. Kessler, J. Spatz, Impact of local versus global ligand density on cellular adhesion, Nano Lett. 11 (4) (2011) 1469–1476.
[15] C. Selhuber-Unkel, M. López-García, H. Kessler, J.P. Spatz, Cooperativity in adhesion cluster formation during initial cell adhesion, Biophys. J. 95 (11) (2008) 5424–5431.
[16] E. Mussig, T. Steinberg, S. Schulz, J. Spatz, J. Ulmer, N. Grabe, A. Kohl, G. Komposch, G. Tomakidi, Connective-tissue fibroblasts established on micropillar interfaces are pivotal for epithelial-tissue morphogenesis, Adv. Funct. Mater. 18 (2008) 2919–2929.
[17] J. Fu, Y.-K. Wang, M. Yang, R. Desai, X. Yu, Z. Liu, C. Chen, Mechanical regulation of cell function with geometrically modulated elastomeric substrates, Nat. Methods 7 (9) (2010) 733–736.
[18] L. Dickinson, D. Rand, J. Tsao, W. Eberle, S. Gerecht, Endothelial cell responses to micropillar substrates of varying dimensions and stiffness, J. Biomed. Mater. Res. A 100 (6) (2012) 1457–1466.
[19] A. Metzner, U. Stock, K. Iino, G. Fischer, T. Huemme, J. Boldt, J. Braesen, B. Bein, J. Renner, J. Cremer, G. Lutter, Percutaneous pulmonary valve replacement: autologous tissue-engineered valved stents, Cardiovasc. Res. 88 (3) (2010) 453–461.
[20] A. Andukuri, M. Kushwaha, A. Tambralli, J. Anderson, D. Dean, J. Berry, Y. Sohn, Y. Yoon, B. Brott, H. Jun, A hybrid biomimetic nanomatrix composed of electrospun polycaprolactone and bioactive peptide amphiphiles for cardiovascular implants, Acta Biomater. 7 (1) (2011) 225–233.
[21] S. Sell, M. McClure, K. Garg, P. Wolfe, G. Bowlin, Electrospinning of collagen/biopolymers for regenerative medicine and cardiovascular tissue engineering, Adv. Drug Deliv. Rev. 61 (12) (2009) 1007–1019.
[22] S. Hinderer, J. Seifert, M. Votteler, N. Shenb, J. Rheinlaender, T. Schäffer, K. Schenke-Layland, Engineering of a bio-functionalized hybrid off-the-shelf heart valve, Biomaterials 35 (7) (2014) 2130–2139.
[23] A. Gaharwar, M. Nikkhah, S. Sant, A. Khademhosseini, Anisotropic poly (glycerol sebacate)-poly (epsilon-caprolactone) electrospun fibers promote endothelial cell guidance, Biofabrication 7 (1) (2015).
[24] S. Alavi, W. Liu, A. Kheradvar, Inflammatory response assessment of a hybrid tissue-engineered heart valve leaflet, Ann. Biomed. Eng. 41 (2013) 316–326.
[25] R. Lima de Miranda, C. Zamponi, E. Quandt, Micropatterned freestanding superelastic TiNi films, Adv. Eng. Mater. 15 (1–2) (2013) 66–69.
[26] U. Stock, I. Degenkolbe, T. Attmann, K. Schenke-Layland, S. Freitag, G. Lutter, Prevention of device-related tissue damage during percutaneous deployment of tissue-engineered heart valves, J. Thorac. Cardiovasc. Surg. 131 (6) (2006) 1323–1330.
[27] J. Boldt, G. Lutter, J. Pohanke, G. Fischer, J. Schoettler, J. Cremer, A. Metzner, Percutaneous tissue-engineered pulmonary valved stent implantation: comparison of bone-marrow derived CD133+-cells and cells obtained from carotid artery, Tissue Eng. 19 (2013) 363–374.
[28] R. Unger, K. Peters, M. Wolf, A. Motta, C. Migliaresi, C. Kirkpatrick, Endothelialization of a non-woven silk fibroin net for use in tissue engineering: growth and gene regulation of human endothelial cells, Biomaterials 25 (21) (2004) 5137–5146.
[29] M. Scherge, S. Gorb, Biological Micro- and Nanotribology, Springer, Heidelberg, 2001.
[30] M. Wohlschlögel, R. Lima de Miranda, A. Schüßler, E. Quandt, Nitinol: tubing versus sputtered film—microcleanliness and corrosion behavior, J. Biomed. Mater. Res. B (2015).
[31] D. Discher, P. Janmey, Y. Wang, Tissue cells feel and respond to the stiffness of their substrate, Science 310 (5751) (2005) 1139–1143.